energies

MDPI

Article

Development of Low-Cost c-Si-Based CPV Cells for a Solar Co-Generation Absorber in a Parabolic Trough Collector

Elsen Aydin [1,2], Armin Buchroithner [3,*], Richard Felsberger [3], Rupert Preßmair [3], Ahmet Azgın [4,5], Rasit Turan [1,4], Ahmet Emin Keçeci [1,5], Gence Bektaş [1,5] and Bulent Akinoglu [1,4,6]

1 Center for Solar Energy Research and Applications (GÜNAM), Middle East Technical University (METU), Ankara 06800, Turkey; elsen.aydin@odtugunam.org (E.A.); turanr@metu.edu.tr (R.T.); gencebektas@gmail.com (G.B.)
2 Department of Archaeometry, Middle East Technical University (METU), Ankara 06800, Turkey
3 Institute of Electrical Measurement and Sensor Systems (EMS), Graz University of Technology, 8010 Graz, Austria
4 Department of Physics, Middle East Technical University (METU), Ankara 06800, Turkey
5 Department of Micro and Nanotechnology, Middle East Technical University (METU), Ankara 06800, Turkey
6 Earth System Science Program, Middle East Technical University (METU), Ankara 06800, Turkey
* Correspondence: armin.buchroithner@tugraz.at; Tel.: +43-316-873-30514

Abstract: Concentrator photovoltaics (CPVs) have demonstrated high electrical efficiencies and technological potential, especially when deployed in CPV–thermal (CPV-T) hybrid absorbers, in which the cells' waste heat can be used to power industrial processes. However, the high cost of tracking systems and the predominant use of expensive multi-junction PV cells have caused the market of solar co-generation technologies to stall. This paper describes the development and testing of a low-cost alternative CPV cell based on crystalline silicone (c-Si) for use in a novel injection-molded parabolic hybrid solar collector, generating both, photovoltaic electricity and thermal power. The study covers two different c-Si cell technologies, namely, passive emitter rear contact (PERC) and aluminum back surface field (Al-BSF). Simulation design and manufacturing are described with special attention to fingerprinting in order to achieve high current carrying capacities for concentrated sunlight. It was determined that Al-BSF cells offer higher efficiencies than PERC for the considered use case. Solar simulator tests showed that the highly doped 4 cm^2 cells (50 ohm/sq) reach efficiencies of 16.9% under 1 sun and 13.1% under 60 suns at 25 °C with a temperature coefficient of −0.069%(Abs)/K. Finally, options to further improve the cells are discussed and an outlook is given for deployment in a field-testing prototype.

Keywords: concentrator photovoltaics; hybrid solar absorber; solar cogeneration; parabolic trough; low-cost solar cells

Citation: Aydin, E.; Buchroithner, A.; Felsberger, R.; Preßmair, R.; Azgın, A.; Turan, R.; Keçeci, A.E.; Bektaş, G.; Akinoglu, B. Development of Low-Cost c-Si-Based CPV Cells for a Solar Co-Generation Absorber in a Parabolic Trough Collector. *Energies* **2024**, *17*, 2890. https://doi.org/10.3390/en17122890

Academic Editor: Rosario Carbone

Received: 28 March 2024
Revised: 21 May 2024
Accepted: 29 May 2024
Published: 12 June 2024

1. Introduction

Without doubt, solar power is an essential part of the energy revolution, with applications ranging from rather innovative approaches, such as direct hydrogen production and sustainable aviation fuels [1,2], to well established systems that supply either heat or electricity. Conventional flat-plate photovoltaic (FPV) modules are commonly used in utility-scale power plants (also on single- or dual-axis trackers) or in residential rooftop PVs. Concentrator photovoltaic (CPV) technology focuses the solar flux on a PV cell to produce electricity directly [1]. CPV-T hybrid systems combine electric and thermal energy generation by using the waste heat of CPV cells, resulting in higher system efficiencies, reduced cell surface area and lower cost at even higher energy yields [3,4]. With its potential to disrupt the solar energy market, once sufficiently high technological readiness levels (TRLs) are reached, CPV-T offers versatile applications for industrial processes [5] and residential applications, such as water purification, the textile industry, building cooling, and heating (Figure 1) [6].

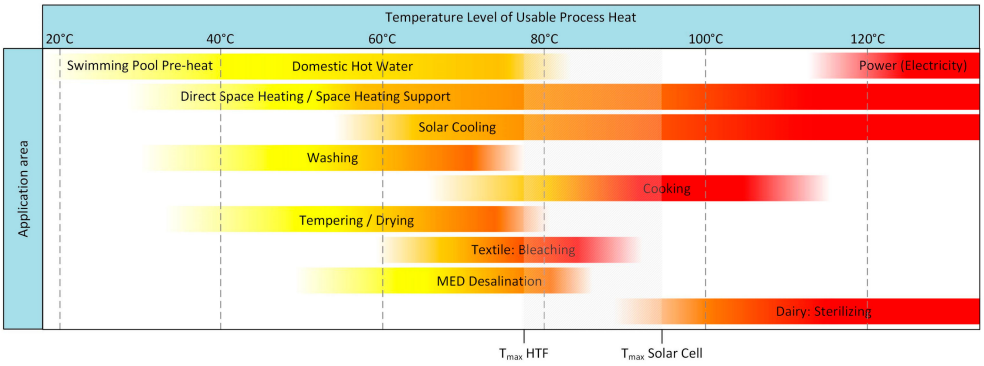

Figure 1. Temperature levels of usable process heat systems for different industrial and domestic solar heat use applications. The approximate operating temperature range of the c-Si CPV cell and its corresponding heat transfer fluid (HTF) temperature is also indicated.

Concentrating solar power (CSP) plants have been installed in various countries [7,8], but their number and cumulative power capacity on a global scale have so far remain limited. Four main types of CSP technologies are worth noting: parabolic trough, linear Fresnel, parabolic dish, and power tower (i.e., central receiver) [9]. Solar power towers (Figure 2a) offer the advantage of reaching very high concentration factors and temperatures, but CPV cells have mainly been applied to parabolic troughs (Figure 2c) or parabolic dish concentrators (Figure 2b), as also described in [10–13].

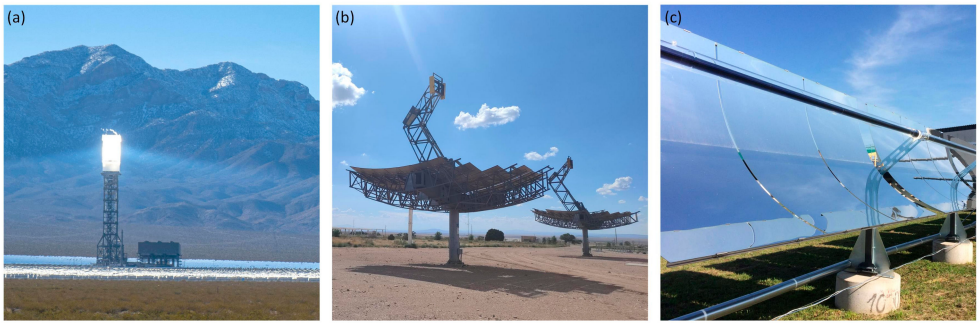

Figure 2. (**a**) Solar power tower, California, USA. (**b**) Parabolic dish concentrator, New Mexico, USA. (**c**) Parabolic trough concentrator by IMK GmbH—Solarmirrortec for district heating, Austria.

One of the main challenges in CPV technology is the high cell's potentially high operating temperatures, which can lead to reduced solar cell efficiency and rapid degradation [2]. Hence, there is a trade-off between PV cell service life and HTF temperature level, which must be considered.

This paper presents the development and testing of a low-cost alternative CPV cell based on crystalline silicone (c-Si) for use in a novel injection-molded parabolic trough hybrid solar collector. Following a state-of-the-art analysis and evaluation of potential use cases for CPV-T heat and electricity generation, target properties for the c-Si PV cell are defined. The development of the cell, including simulation and manufacturing, is described in detail. Solar simulator tests demonstrate that the CPV cell can achieve efficiency of 16.9% under 1 sun concentration at 25 °C and 13.1% at 60 sun concentration at 35 °C, with a temperature coefficient of −0.069%(Abs)/K. The procedures and results are discussed in depth. The development process of the c-Si CPV cell presented in this paper is summarized in the graphical abstract provided alongside this publication.

This research was conducted as part of a SOLAR-ERA.NET project involving partners from academia and industry in Austria, Spain, and Turkey, with Middle East Technical University Center for Solar Energy Research and Applications (ODTÜ-GÜNAM) responsible for the solar cell design.

2. Motivation and State of the Art

While CPV-T systems have demonstrated high overall efficiencies, their cost is still significantly higher than flat-plate alternatives. This can be explained by the increased complexity (e.g., tracking [14] secondary optics [15], etc.) and higher cost of the often used CPV multi-junction cells [16,17]. Though promising and intriguing, some of the proposed systems, such as [18] rely on a rather large number of optical components. Despite their great technological potential, both CPV and CPV-T (i.e., solar thermal and electric co-generation in concentrating solar power (CSP)) have not yet achieved significant economic success compared to their less efficient counterparts, such as conventional c-Si PV modules and solar thermal collectors. Two of the main shortcomings of CPV and CSP lie in the increased system complexity and higher installation cost. Furthermore, concentrating systems require direct irradiance and cannot effectively use diffuse radiation, making them less suitable for high latitude and frequently cloudy installation sites.

The goal of this work is to reduce the cost of all components involved in a parabolic trough CPV-T hybrid system, i.e., support structure, concentrating elements, e.g., mirrors, tracking mechanism, solar cell, heat sink, etc. and design a system that is easy to assemble and adjust in the field.

In CPV applications, mainly high-cost, high-performance multi-junction solar cells [6,10] or GaAs-based cells [13] are used, which rely on limited and rather expensive raw materials. Hence, in order to advance CPV-T technology, low-cost alternatives based on abundant materials such as Si must be considered, as previously argued in [10]. Therefore, this research is focused on designing and producing suitable c-Si CPV cells, which must be capable of operating under concentration factors of around 60 suns and withstand local peaks of 150 suns.

The CPV-T system prototype, as shown in Figure 3, was intended to power an absorption chiller for an industrial building cooling application. The application itself is key for determining the c-Si CPV cell's requirement profile, as it determines not only the electrical power and energy need but also the necessary temperature levels.

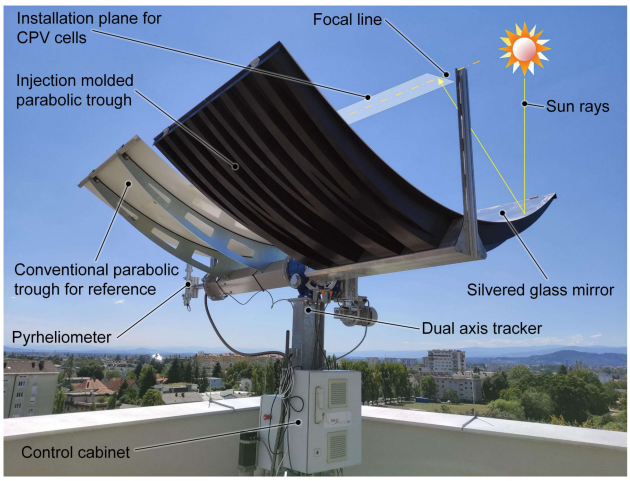

Figure 3. Overview of the parabolic trough CPV system showing the mounting position of the CPV cells developed and presented within the scope of this publication.

3. Development of a Low-Cost c-Si CPV Cell

3.1. General System Layout

Solar cell design involves determining the target parameters of the solar cell structure to maximize efficiency given a certain set of constraints, which are defined by the operating environment and the application itself. If the goal is to produce a competitively priced solar cell, the cost of producing a particular structure in a commercial setting where the cells will be installed must be considered. However, if the goal is to produce a high-performance laboratory cell, operated in a research setting, optimizing efficiency rather than cost would

be the main goal. Therefore, in this study, a c-Si based solar cell is designed with an emphasis on maximum cost reduction.

The cells are part of a so called co-generation absorber module (CAM), which is placed in the PTC instead of a conventional tube collector. The prototype CAM consists of a heat sink in the form of a metallic tube, containing the heat transfer fluid (HTF) and a solar "cell tray" attached to the tube by spring-loaded CPV module mounts. The absorber tube and the cell tray (see Figure 4) are placed in the focal line of the PTC, as shown in Figure 3.

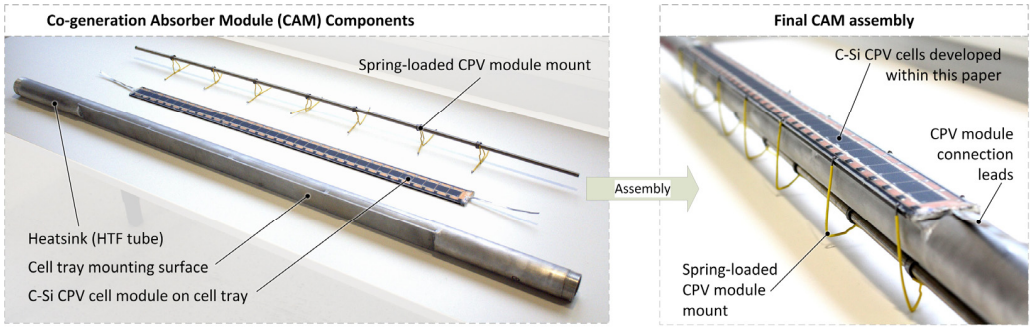

Figure 4. Co-generation absorber module (CAM) components and prototype assembly.

3.2. CPV Cell Development Steps

The first parameter taken into consideration is the cell front surface metal contacts, also referred to as "finger design". The role of the front surface metal finger contacts is to transfer the electrical current with minimal ohmic losses, while at the same time occupying as little space on the cell's front surface as possible to minimize shading. Front surface metal contact design is especially critical for CPV cells because they produce higher currents than regular PV cells.

Preliminary studies were carried out to generate an elaborate requirement profile. This was necessary to find the optimal cell design by using an iterative approach for the target operating temperature of 90 °C at a concentration factor of roughly 60 suns. Front metallization design (finger shape, space between two fingers, finger length, and width) was optimized for highest lateral conductivity and lowest shading in order to improve saturation current (J_{SC}) and fill factor (FF).

The effect of J_{SC} on solar cell performance under high concentrations is investigated experimentally after actual cell production. The main steps of the design process were:

1. Front side metal design.
2. Heat-sink integration requirements.
3. Resistance loss analysis.
4. Tests for validation toward simulated targets.

In order to maximize efficiency, the design process of the envisioned single junction c-Si solar cell pursued the following goals:

- Enhancing the quantity of light gathered by the cell converted into carriers (as in [1]).
- Increasing the aggregation of light-generated carriers by the p–n junction.
- Transporting current from the cell without considerable resistance losses.

3.3. Target Specifications and Design Requirements

The focal point of a concentrating solar system (or focal line of a PTC, for that matter) does not feature perfectly uniform flux distribution due to the real-world physical properties of optical components (e.g., reflecting surfaces, lenses, mirrors). Since the flux distribution depends on the concrete system design and on many physical and material uniformity properties, its exact determination can be a complex undertaking, as was also shown in [9] and is also discussed, for instance, in [19]. However, the flux distribution can be approximated by a Gaussian curve, as shown in Figure 5, if no secondary optics are deployed, as was the case in [20].

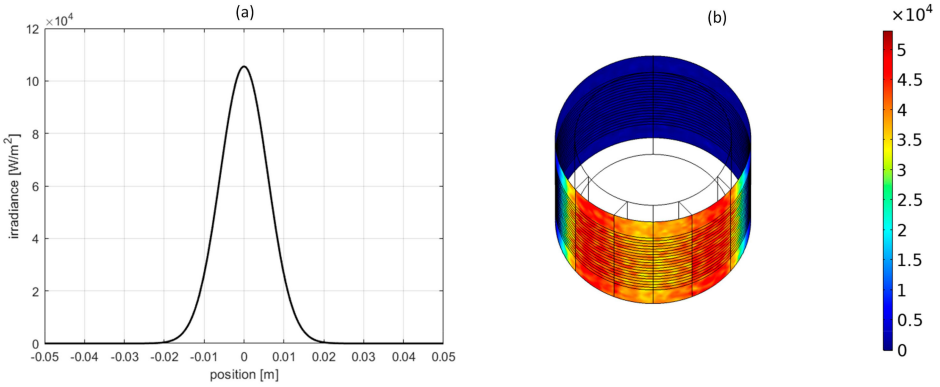

Figure 5. (**a**) Gaussian flux distribution of an ideal parabolic mirror with a 2.2 m aperture on a flat target plane. (**b**) Comparison with simulation conducted in COMSOL for a 40 mm-diameter thermal absorber tube in the same parabolic trough collector.

The "width" and exact shape of the flux distribution depend on a variety of parameters and the CPV cell needs to be designed accordingly. A general rule of thumb applies, though: the lower the concentration factor, the larger the active cell area needs to be in order to provide the same electrical power output (and vice versa). The precise placement of the cell in terms of the focal distance (i.e., its position relative to the parabolic mirror) also plays a role, as was demonstrated in [9].

In the design envisaged for the co-generation absorber module (CAM), the CPV cell will be placed on a tubular heat sink carrying the heat transfer fluid (HTF), which has a double purpose:

(a) Cooling the backside of the solar cell.
(b) Conveying the rejected heat for subsequent use in an absorption chiller or similar.

Different cell sizes were considered to find the most suitable cell dimensions for integration into the CAM. The production stages will be discussed in the following section.

Eventually, a cell width of 2 cm was chosen based on in order to ensure that the cells matched the Gaussian flux distribution shown in Figure 5.

4. CPV Simulation for Cell Design

4.1. c-Si Cell Architecture

A typical silicon solar cell consists of a thin layer of the phosphor-doped (n-type) silicon in the surface region of the boron-doped (p-type) silicon wafer. The p–n junction creates an electric field that provides the main mechanisms to separate the electron–hole pairs upon optical absorption. When sunlight hits the surface of a PV cell, the light-excited electrons gain momentum, causing a current flow [4].

The optimization of metallization (i.e., finger and busbar manufacturing) under 1 sun was studied assuming uniform light distribution and taking into account earlier work [6]. There have also been studies to design efficient metallization for certain solar cell geometries under higher concentrations with uniform light distribution [10,11].

4.2. Front Surface Metallization Design

In this section, front surface metallization design and optimization for concentrated lighting conditions via simulation software Griddler 2.5 PRO and Quokka v2.2.5 are described. The goal was to optimize all relevant elements of the CPV cell and their non-uniform lighting profiles and to assess the current density and voltage distribution throughout the cell.

CPV systems use optical elements such as reflectors (mirrors, etc.) or collectors (lenses, etc.) to concentrate the light flux on the solar cells [13]. Thus, the incoming light is "intensified" at a certain rate, the so-called concentration ratio, to increase the power output at a given cell area. In the case of a typically non-uniform, Gaussian-like flux distribution

(compare Figure 5), the current density and temperature increase locally in the cell, which may cause higher voltage to drop and increased ohmic losses. In addition, it is known that the series resistance created by this non-uniform lighting causes a serious decrease in power output [13,21]. One way to minimize these losses is to improve the uniformity of the metallization of the solar cell for the given illumination and temperature profile.

One of the most important effects on efficiency of PV cells is the ohmic resistance that occurs within the cell (see Figure 6). Especially in the case of concentrator photovoltaics, the resistances become critically important for the performance. Current leakage increases with concentration factor in an exponential manner, due to changes in physical parameters like temperature increase, etc. [22]. The exponential correlation can be seen in Formula (1):

$$I_0 = qA\frac{D}{LN_D}BT^3 exp(\frac{E_{G0}}{kT}) \approx B'T^{\gamma} exp(-\frac{E_{G0}}{kT}) \quad (1)$$

q: electric charge
A: area
D: diffusivity of the minority carrier
L: minority carrier diffusion length
N_D: doping coefficient
B: temperature-independent constant
T: temperature
k: Boltzmann's constant
E_{G0}: bandgap linearly extrapolated to absolute zero
B': temperature independent constant
γ: factor regarding temperature dependencies of the other material parameters.

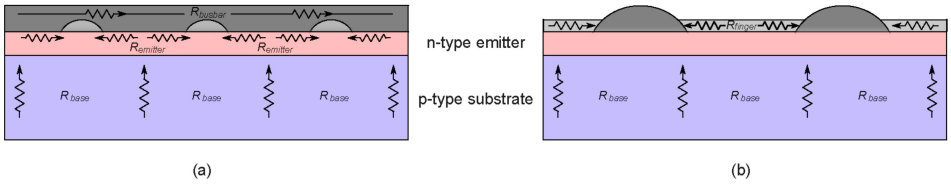

Figure 6. Schematic representation: (**a**) front view (**b**) side view of series resistances of a solar cell—$R_s = R_{emitter} + R_{base} + R_{finger} + R_{busbar}$.

The cumulative resistance losses within the cell are defined as the characteristic resistance (R_C) consisting of various components, as illustrated in Figure 6.

The individual parasitic losses, which create the cumulative resistance for CPV solar cells can be examined under the main resisting parts, namely:

- Series resistance (R_S).
- Shunt resistance (R_{SH}).
- Contact resistance ($R_C = R_{finger} + R_{busbar}$).

The series resistance of a solar cell is an ohmic resistance that causes a decrease in the fill factor (FF) and is usually grouped as series resistance R_S. In CPV cells, high irradiance (and consequently higher current and operating temperature) causes higher voltage drops and increased ohmic losses. In addition, it is known that the series resistance created by this non-uniform lighting causes a serious decrease in the power output [13]. One way to minimize these losses is to improve the uniformity of the metallization of the solar cell for the given illumination and temperature profile.

The magnitude of the shunt resistance R_{SH} is an indicator of the current leakage in the solar cell, as it measures how effectively the solar cell can prevent current from bypassing the intended electrical path. This leakage can originate from various sources, primarily from imperfections on the edges of the solar cell and potentially due to flaws in the p–n junction. Furthermore, additional current leakage can occur at the points where the cell's

surface connects with the metallic fingers and base. These factors collectively contribute to a short circuit that results in unwanted current leakages.

Contact resistance R_C is formed between the front side metal printing of the solar cells, the fingers and the emitter region. To reduce this resistance, the emitter must be heavily doped. If heavy doping is applied during cell manufacturing (and low emitter sheet resistance is achieved), good contact formation will result due to the increased conductivity of the emitter. In addition, heavy doping minimizes the specific R_C, which is desired for low series resistance in a solar cell. Contact quality is greatly affected by the firing process (crucial manufacturing step during which the front metal contact is formed in c–Si solar cell to dry the solvent of metallic paste), which is described in more detail in Section 5. For this reason, it is necessary to increase the contact quality by making appropriate firing scans and optimizing the furnace temperatures.

Series, shunt, and contact resistances are important specifications for the cells presented in this paper. Manufacturing of the cells was performed at the ODTÜ-GÜNAM Photovoltaic Line (GPVL). Preliminary evaluation was conducted via simulations with Griddler 2.5 PRO initially pursuing the architecture of an industrial passive emitter rear cell (PERC) under concentration. The results for short-circuit current (J_{SC}) versus open-circuit voltage (V_{OC}) are given in Figure 7.

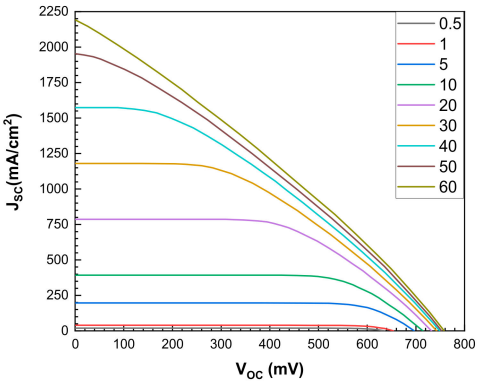

Figure 7. *J–V* curves for an initially investigated PERC cell with concentration factors ranging from 0.5 to 60 suns, simulated in Griddler 2.5 PRO.

In this simulation, it was also found that the fill factor (FF) decreases as the concentration factor increases, leading to a decrease in cell efficiency. This trend can also be seen in Figure 7, which shows J_{SC}–V_{OC} curves for an industrial PERC solar cell with concentration factors ranging from 0.5 to 60 suns. The effects of the concentration values on efficiency and variation between V_{OC} and J_{SC} are shown in the graphs below (see Figure 8).

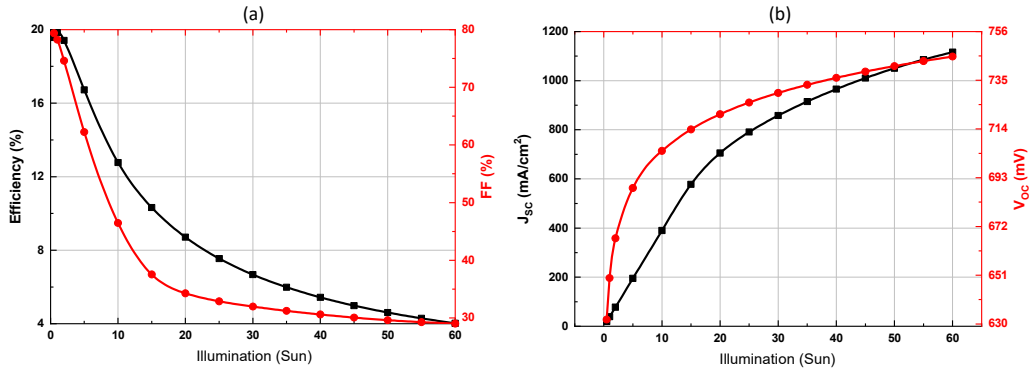

Figure 8. (**a**) Variation of efficiency and FF and (**b**) J_{SC} and V_{OC}, simulated in Griddler 2.5 PRO.

As shown in Figure 8a, the efficiency decreases exponentially to about 4%, while the fill factor (FF) decreases to 30%. As expected and illustrated in Figure 8b, the short-circuit

current (J_{SC}) and open-circuit voltage (V_{OC}) increase with increasing solar flux on the cell. The geometric model of the cells was initially designed in AutoCAD 2020, then transferred to Griddler 2.5 PRO and simulated under 60 sun concentration. The decision to use PERC technology for the envisioned CPV module was based on the typically higher V_{OC} values, which usually lie above 650 mV.

Since the dimensions of the CPV cells were determined based flux distribution (also see [23] and Figure 5), the optimization process began with the front surface metal design. For optimization, the number of fingers and busbar design take priority as an H-pattern metallization design was chosen. The utilization of an H-pattern metallization is a strategic choice was driven by several key factors in the context of simulating solar cells, as discussed in prior research [24,25]. Its symmetrical and repeating structure enables the reproduction of identical regions, offering a valuable means of validating simulation results across the entire cell. Moreover, the H-pattern plays a crucial role in minimizing edge effects within the emitter section, which can introduce variations or anomalies near the cell's boundaries. By encompassing the entire emitter with this pattern, any numerical challenges or irregularities that arise near the edges can be consistently assessed and addressed, ensuring the accuracy and reliability of the simulation process.

In the proposed design, the wafer is attached to a busbar and the fingers are placed perpendicularly. This design choice aims to ensure that the high current produced by the solar cell under concentration is carried with minimal ohmic losses. However, to achieve the highest electrical efficiency, it is crucial to maximize the active area of the cell relative to its overall size. As a result, the busbar and finger placements of the PERC cells must be designed to align with this objective. To optimize the number of fingers, the simulation results under 1 sun and 60 suns were compared. It is observed that a finger width of 40 µm resulted in the highest performance under concentrated sunlight of 60 suns. The finger parameters obtained are given in Table 1.

Table 1. The physical parameters obtained for fingers and busbar of the planned CPV cell.

Property	Value	Unit
Finger sheet resistance	0.2	mohm/sq
Finger contact resistance	1	mohm-cm^2
Emitter sheet resistance	50	ohm/sq
Finger width	40	µm
Busbar width	2	mm

In Figures 9 and 10, the results for efficiency, FF, J_{SC}, and V_{OC} of the CPV cell under 1-sun and 60-sun concentrations are depicted. Standard 15.6 × 15.6 cm industrial cells produced at the GÜNAM PV line use 86 fingers, which is why this value was chosen as a starting point. However, the highest efficiencies were obtained with a finger number of 121 for the investigated use case. Under 1 sun, J_{SC} is decreasing with increasing finger number, while V_{OC} remains nearly the same, as shown in Figure 9b on the right. However, for 60 suns, both J_{SC} and V_{OC} are increasing, as shown in Figure 9a on the left.

The observed improvement in efficiency when using 121 fingers in the CPV cell design under 60 suns of solar concentration can be attributed to a notable increase in the electric current generated by the cell. Under these highly concentrated sunlight conditions, a greater number of photons strike the cell, exciting more electrons and leading to a substantial rise in the short-circuit current (J_{SC}). This increase in current, when combined with other parameters such as voltage (V_{OC}) that remain relatively constant or even increase, contributes to the overall enhancement in efficiency. The utilization of 121 fingers in the cell design appears particularly effective in this high-concentration scenario, likely optimizing electron collection and minimizing losses, ultimately resulting in superior overall performance for the CPV cell in high solar flux conditions. Also, it must be noted that the FF decreases under 60 suns while under 1 sun it increases, as shown in Figure 10.

The effect of finger sheet resistance R_{SH} and finger contact resistance R_C on efficiency was evaluated under 60-sun concentration. Again, the optimization was conducted in Griddler 2.5 PRO and the results obtained are given in Figure 11.

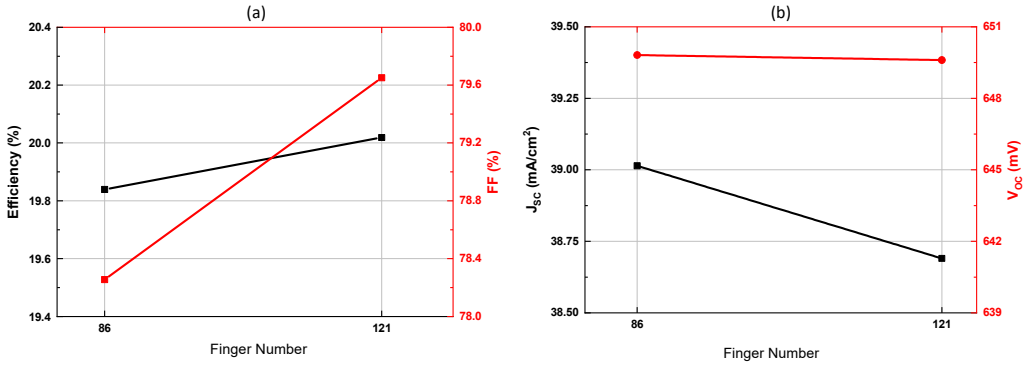

Figure 9. CPV cell finger optimization for 1 sun obtained by preliminary simulation with Griddler 2.5 PRO. (**a**) Efficiency (%) and fill factor (FF) (%) versus finger number and (**b**) Short-circuit current density (J_{SC}) (mA/cm²) and open-circuit voltage (V_{OC}) (mV) versus finger number.

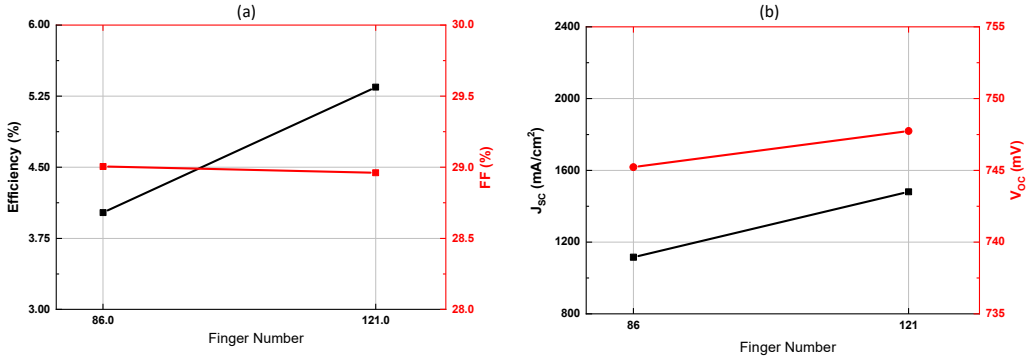

Figure 10. CPV cell finger optimization parameters for 60 sun obtained by preliminary simulation with Griddler 2.5 PRO. (**a**) Efficiency (%) and fill factor (FF) (%) versus finger number and (**b**) Short-circuit current density (J_{SC}) (mA/cm²) and open-circuit voltage (V_{OC}) (mV) versus finger number.

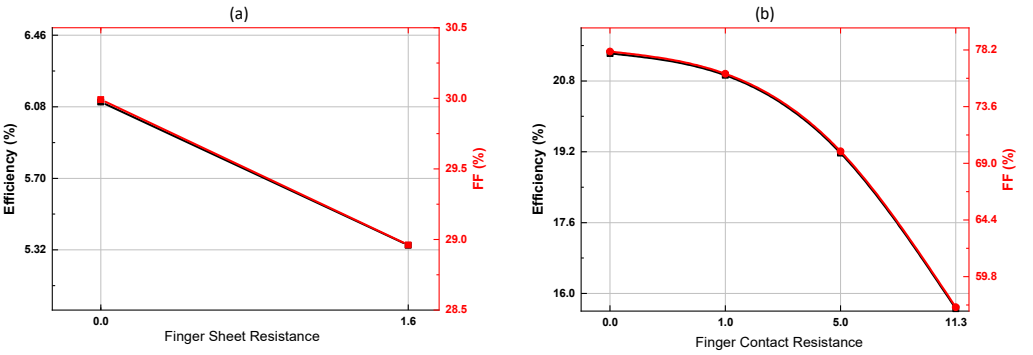

Figure 11. (**a**) Plot of efficiency and FF versus increasing finger resistance under 60-sun concentration. (**b**) Plot of efficiency and FF versus increasing finger contact resistance under 60-sun concentration.

As expected, an increase in finger sheet resistance and finger contact resistance results in a reduction in efficiency and fill factor (FF). The solar cell designed, with a width of 2 cm, was evaluated under 60-sun concentration using the graphics presented above and simulated using the values provided in Table 2.

Table 2. Simulation result of CPV cell of 5 × 2 cm^2 under 60 suns.

Wafer Length (cm)	Wafer Width (cm)	Finger Number -	J_{SC} (mA/cm^2)	V_{OC} (mV)	Fill Factor (%)	Efficiency (%)
5	2	100	2261.6	730.4	81.6	22.5

J–V curve simulations in Quokka v2.2.5 were carried out for both PERC and Al-BSF cells, as shown in Figure 12.

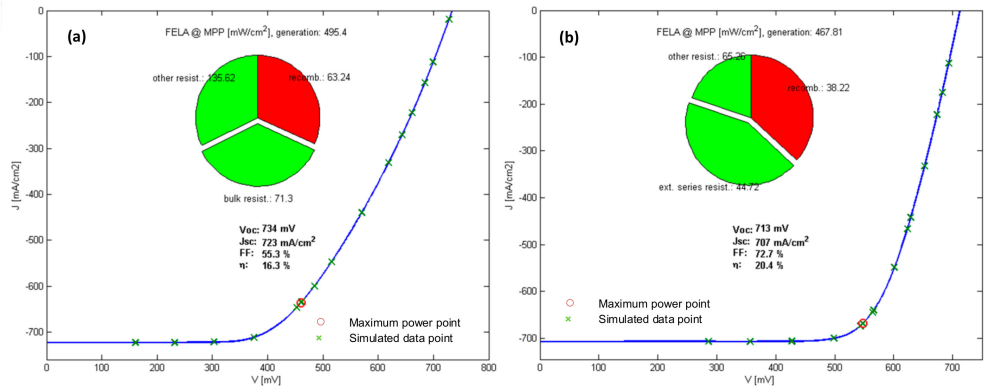

Figure 12. Quokka v2.2.5 simulation results in terms of current density-voltage (J-V) characteristics and resistance analysis at the maximum power point (MPP) for (**a**) PERC cell (**b**) Al-BSF cell.

According to the simulation results, there is a significant decrease in the fill factor (FF) in PERC cells when compared to Al-BSF cells. Al-BSF cells were also used in subsequent cell production, similar to PERC cells, and a comparative analysis was conducted with a focus on performance under solar flux concentration, as described in the next section.

5. Manufacturing

Manufacturing of the cells described above was carried out at ODTÜ-GÜNAM GPVL in Ankara, Turkey. The steps of PERC cell production are summarized in Figure 13 (left), and the production line is shown on the right.

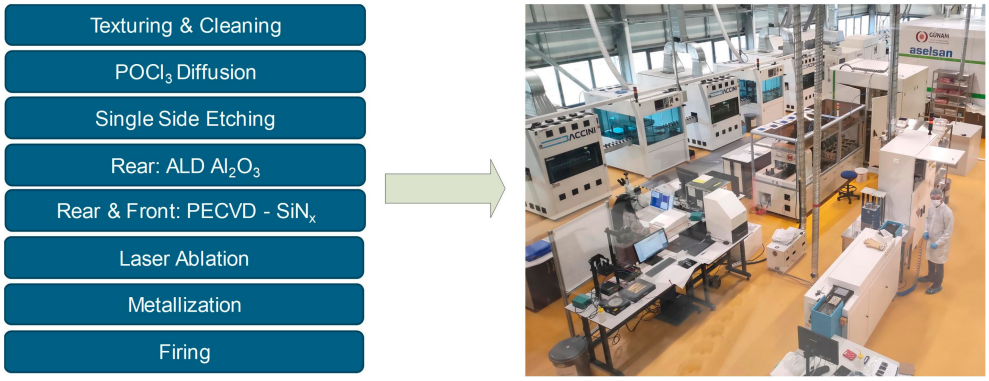

Figure 13. Process flow of PERC cell (**left**) manufacturing at GÜNAM GPVL (**right**).

After texturing and cleaning, phosphorus doping was applied in order to reach the targeted spreader plate resistance. Doping was performed at 830 °C for 7 min. Both surfaces of doped c-Si slices were then coated with a PECVD-SiNx layer at 450 °C for 20 min before and after metal printing.

After nitrate coating, screen printing was carried out with the help of metal masks. Because of its low cost, high throughput and simplicity, the well-established "screen printing method" was used for metal-on-cell printing during c-Si cell production [26]

and Applied Baccini Cell Systems is used for screen printing at GPVL. Using simulation results, the screen mask was designed with a finger width of 30 µm so that considering the dispersion of the silver paste after screen printing, an actual finger of approximately 40 µm was reached. The Al-SBF cell process flow is summarized below in Figure 14.

Figure 14. Process flow of Al-BSF cell production.

The metallization process, which is the last stage of PV cell production, is one of the most important steps for cells that will operate under high solar concentration. The print quality and height of the fingers, which will have to carry high electric current, are crucial. The tightly placed fingers should be as narrow as possible while maximizing their height.

Fingers and busbars were closely examined after the metallization process with an optical microscope to control the quality. Since the fingers are relatively thin, spreading and knuckles were observed in the silver paste during printing. GÜNAM's metallization process line is shown in Figure 15 and metallization optical images of the fingers at different magnifications are given in Figure 16.

Figure 15. Solar cell metallization process.

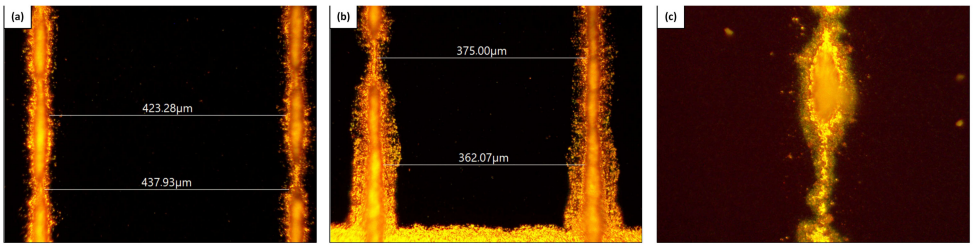

Figure 16. Initial finger printing attempt: optical images of metallic fingers of CPV cell under different optical magnifications. Left to right: (**a**) view of two fingers under 20×, (**b**) two fingers and (**c**) busbar intersection under 20×, finger under 40×.

Double printing was chosen as a method to resolve the now identified issue of knuckling and spreading of the paste and an optical microscope was used for preliminary assessment of the quality of the double print. These images in different magnifications are shown in Figure 17.

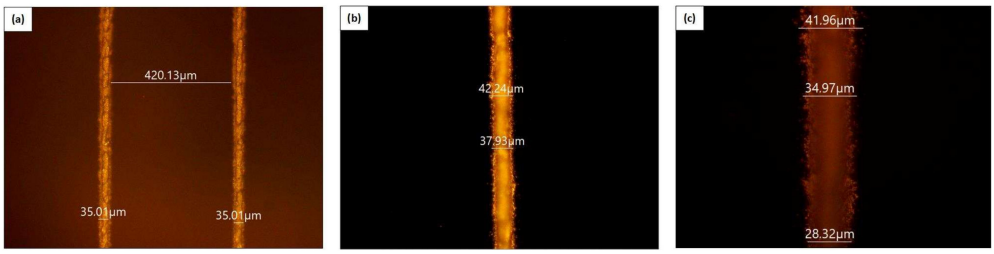

Figure 17. Improved finger printing process: optical images of double prints. Left to right: (**a**) view of two fingers under 40×, (**b**) finger under 20× and (**c**) finger under 40×.

The cells were initially printed using Herause Sol9681B silver paste (Herause Group, Hanau, Germany). However, during the first electrical tests, high shunt resistance values were observed. As a result, the process was changed to printing with float paste—Herause 6600B (Herause Group, Hanau, Germany) [27]. Additionally, a decrease in efficiency was observed in the solar cells due to the region of recombination that formed under the 2 mm-wide busbars. To address this problem and reduce the recombination region, the decision was made to cut the edges of busbars and continue to use them as shown in Figure 18.

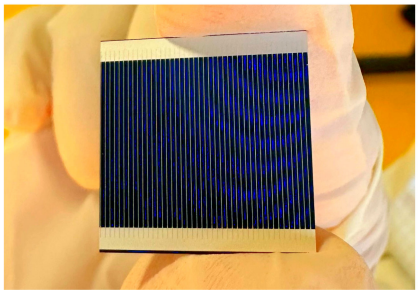

Figure 18. First 2 × 2 cm Al-BSF CPV cell manufactured at ODTÜ-GÜNAM GPVL (edge busbars were cut) with an active cell area of 1.6 × 2 cm.

Initially planned as a 2 × 5 cm cell, the aspect ratio was later changed to 2 × 2 cm to handle the high currents when operating under concentrated sunlight. This change aligns with practical reasoning to reduce ohmic losses and avoid using excessively thick copper wires. In general, it is necessary to achieve a tight packing of cells on the modules (i.e., ideal exploitation of the line focus), which is—in addition to reducing the recombination area—why the busbars were cut on the sides.

6. Test Results

Testing of the cells consisted of experiments performed in the following order:

(a) ECV.
(b) EQE.
(c) 1-sun solar simulator tests.
(d) High-flux solar simulator tests.

ECV (electrochemical capacitance voltage) measurement was conducted to determine the junction depth, EQE (external quantum efficiency) was used to determine surface recombination, and simulator tests under 1 sun were performed on the highly phosphorus-doped cells with 50 ohm/sq sheet resistance (Figure 19). As per the results, the junction depth is 0.50 µm and the junction thickness is 0.56 µm. Based on EQE measurement, the J_{SC} value under 1 sun is 32.671 mA/cm^2.

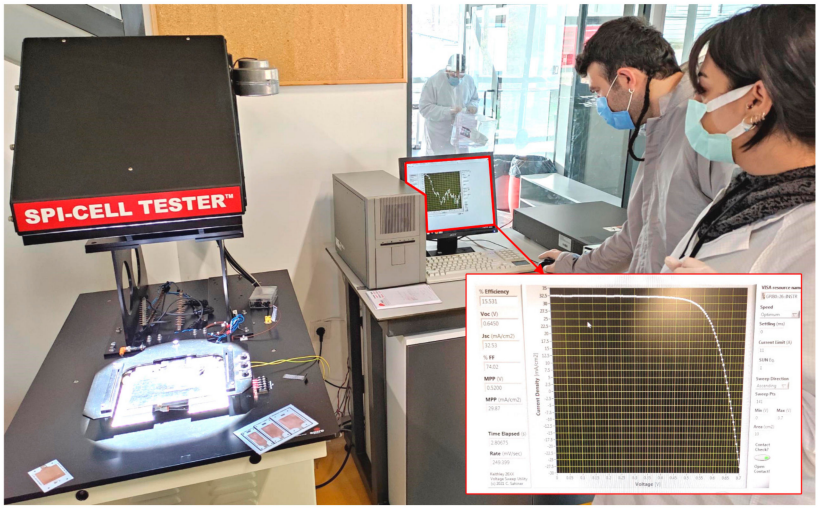

Figure 19. Simulator test using Spi-Cell Tester under 1 sun.

Graphs of ECV and EQE measurements result are given in Figure 20a,b.

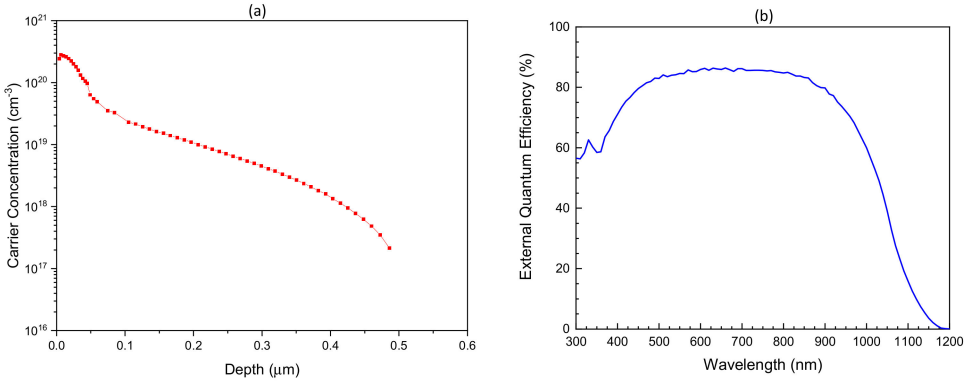

Figure 20. (**a**) ECV and (**b**) EQE measurement results of the 2 × 2 cm Al-BSF cells.

J_{SC} can be calculated from the EQE by integrating the EQE over the entire solar spectrum and then considering the appropriate conversion factors. The AM1.5G solar spectrum is used as the reference spectrum for this integration, as it represents the typical solar spectrum at the earth's surface. The AM1.5G spectrum is defined by the American Society for Testing and Materials (ASTM) standard G173-03 [28] and has a photon flux of 1000 W/m^2 [29].

The calculation of J_{SC} from EQE integrated over the AM1.5G spectrum can be expressed mathematically as:

$$J_{SC} = (q/hc) \times \int [EQE(\lambda) \times AM1.5G(\lambda) \times \lambda]\, d \quad (2)$$

where q is the electron charge (1.602×10^{-19} C), h is the Planck's constant (6.626×10^{-34} Jus), c is the speed of light (2.998×108 m/s), $EQE(\lambda)$ is the external quantum efficiency as a function of wavelength λ, and AM1.5G(λ) is the spectral irradiance of the AM1.5G solar spectrum as a function of wavelength λ. The integral is taken over the entire wavelength range of interest, which means the range over which the solar cell has a non-zero quantum efficiency and hence can effectively absorb and convert photons to electric current.

In practice, the EQE is usually measured using a calibrated spectrophotometer, and the AM1.5G spectrum is often provided by a solar simulator that can produce light with the same spectral distribution as the AM1.5G standard [30]. The measured EQE data are then multiplied by the AM1.5G spectrum and integrated over the wavelength range to obtain J_{SC} [31].

6.1. Rc Measurement Results

In order to measure the contact resistance of the fingers after metal printing, the line resistance in the produced cells was measured using a TLM device by PVtools 1.1.3 [32] and determined to be 0.7135 ohm/cm (Figure 21). For reasons of comparison, the resistance value obtained when measuring with the same method in a commercially available PERC cell [33] was 0.6710 ohm/cm. While the difference between the two values is not large, the reason was assumed to be non-uniformities and imperfections in the printing process.

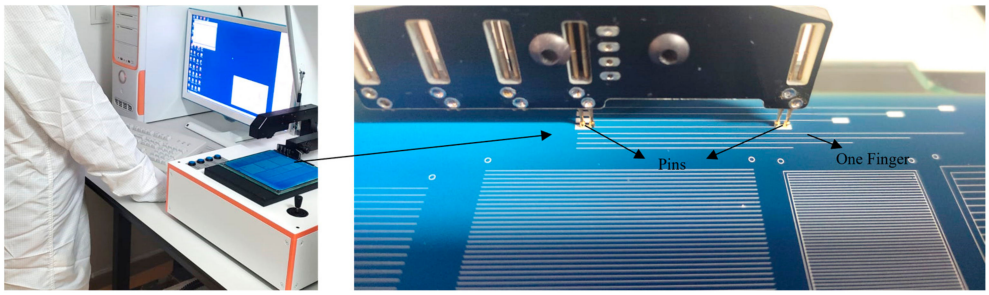

Figure 21. Measurement of line resistance using a TLM device by PVtools.

6.2. Standard Solar Simulator Tests

After the resistance values had been obtained, the cells were characterized in a commercially available 1-sun solar simulator [34], and the results of cell parameters obtained for the first design (i.e., the 2 × 5 cm cell) are given in Figure 22.

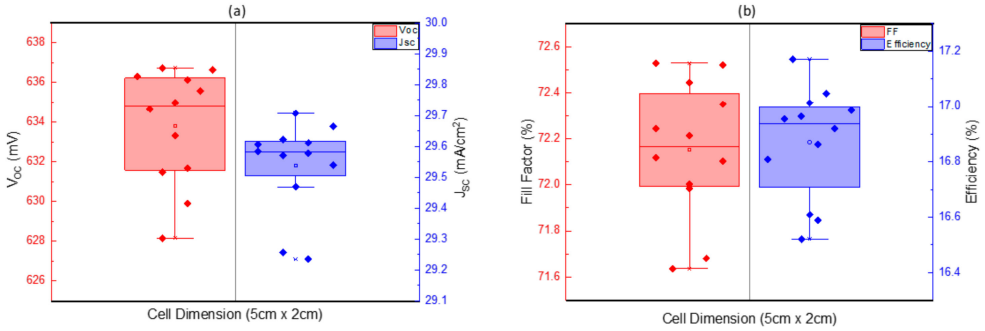

Figure 22. CPV cell parameters under 1-sun solar simulator. (**a**) Short-circuit current density (J_{SC}) (mA/cm²) and open-circuit voltage (V_{OC}) (mV) versus cell dimensions (**b**) Efficiency (%) and Fill Factor (FF) (%) cell dimensions. Each dot represents one cell sample.

After conducting the first physical characterization processes (i.e., ECV and TLM measurements), the cells were tested to determine their light-induced degradation (LID). To begin with, initial V_{OC} (open-circuit voltage) measurements were taken, and the CPV cells were sorted under room conditions and rested for 19 h before the regeneration process. The samples were then subjected to thermal shock by heating them on a hot plate at 200 °C for 10 min and subsequently exposed to 1-sun illumination while being kept at 140 °C for 3 h. Following this, the samples were allowed to stabilize their V_{OC} values for 3 h.

The measurements taken immediately after production and the measurements made after the LID process showed no significant difference. This indicates that no degradation occurred in the CPV cells produced after the LID process was performed. Consequently, it can be concluded that the cells achieved physical stability after LID.

6.3. High-Flux Solar Simulator Tests

After the LID process, the cells were laminated so that measurements could be taken under concentration. Laminating the cell samples prior to solar simulator testing was necessary to avoid thermal distortion and ensure proper backside cooling contact. Aluminum was used as a backside substrate for lamination to ensure that the waste heat of the cells

operating under concentration was effectively rejected to the heat sink in the test setup. The process is shown in Figure 23.

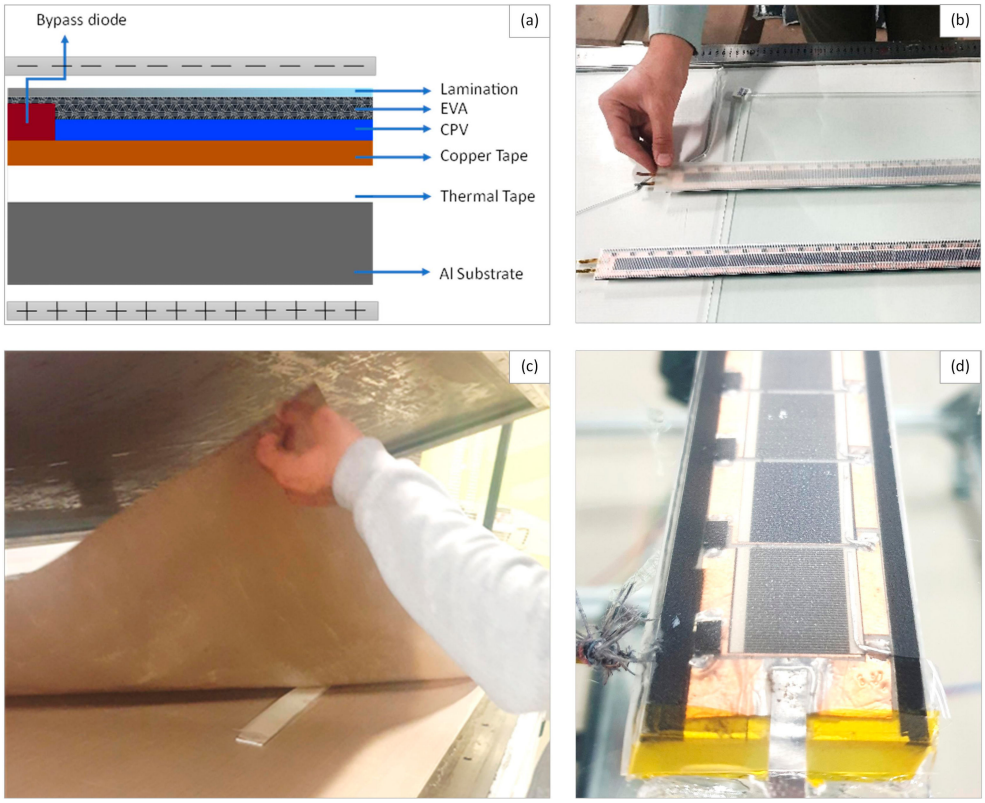

Figure 23. Detailed lamination process. (**a**) Sketch of cross section; (**b**) preparation of lamination; (**c**) lamination process; (**d**) laminated PV array.

The manufactured cells were tested using two independent high-flux solar simulators, one located at ODTÜ-GÜNAM in Turkey and the other at Graz University of Technology (TUG) in Austria. This decision was made to obtain reliable and independent test results and to ensure that possible spectral mismatches of each solar simulator were taken into consideration.

The use of two independent solar simulators helped to ensure that the test results were accurate and reliable. This is particularly important when evaluating the performance of CPV cells, which are designed to operate under concentrated sunlight. The data obtained from these tests can be used to assess the efficiency of the cells and determine their suitability for practical applications.

The main purpose of the simulator at ODTÜ-GÜNAM is for CSP (concentrated solar power) simulations, and it must be noted that this system has not been calibration for solar cell measurements. However, the simulator at TUG has been characterized and is suitable for solar cell measurements, as it adheres to international standards [35]. Therefore, to ensure reliable test results, the simulator at TUG was also used.

6.3.1. Solar Simulator Test at METU

ODTÜ-GÜNAM's high-flux solar simulator uses three Xe-arc lamps, with an electrical power of 6 kW each. Xe-arc lamps are known for their high spectral fidelity to the solar spectrum, making them an ideal light source for solar cell testing [23]. However, when used without an appropriate AM 1.5 filter, the infrared share of the spectrum can be overrepresented, which can be problematic.

During the experiment, the AM 1.5 filter placed in front of the light sources was damaged as it could not handle the high power and temperature of the Xe-arc light sources. As a result, the measurements had to be conducted without the filter, as is shown in

Figure 24. Additionally, the physical design of the AM 1.5 filter, with an output beam diameter of merely 1 cm, is insufficient to accommodate the larger beam size produced by the high-intensity Xe-arc lamps. This mismatch in beam size means that the filter cannot effectively cover and modify the entire light beam emitted by the lamps, further limiting its utility in this context.

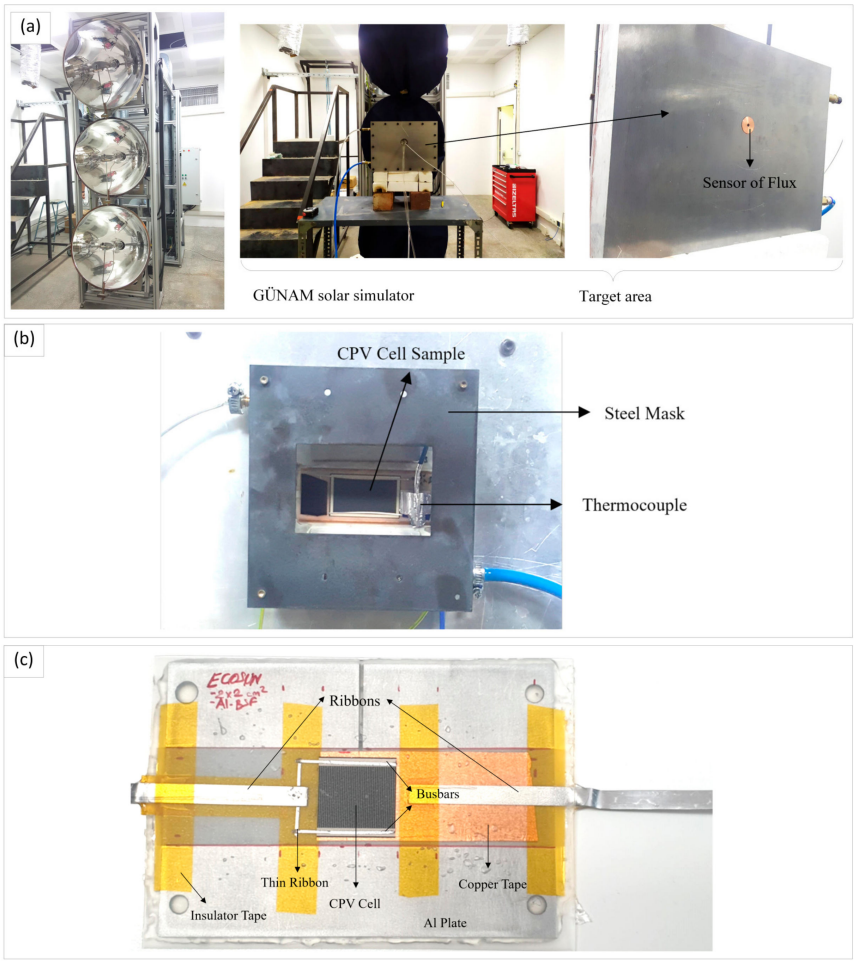

Figure 24. (**a**) Xe-arc concentrator system and sensor of flux distribution. (**b**) CPV cell measurement substrate with heat sink. (**c**) Laminated CPV cell for measurement.

This experience underscores the importance of ensuring compatibility between all components in a high-flux solar simulation system and highlights the challenges involved in accurately simulating solar conditions for such CPV and CSP applications.

Despite this setback, the measurements were still useful in determining the performance of the CPV cells under concentrated sunlight. The data obtained from the experiment, although not entirely ideal, still provided valuable insights into the cells' efficiency and suitability for practical applications.

Figure 25 shows the I–V curve of the Al-BSF cell in comparison to the previously manufactured and PERC cell. The measurements were performed taken at 25 °C and under different concentration factors.

While the I–V curves of both cell technologies reveal that the PERC cell technology has a higher open-circuit voltage, the Al-BSF cell boasts lower series resistance, leading to better performance. The first reason for this is that minority carriers (i.e., electrons) are kept away from the back surface, which is pivotal, as these minority carriers can detrimentally affect the efficiency of the cell if they accumulate at the back. Secondly, when these solar cells operate under higher sunlight concentrations, the Al-BSF ensures that the resistance within the cell material (or the bulk) remains low, which in turn enhances overall performance.

Both in simulations and actual measurements, it was observed that Al-BSF cells exhibited more stable performance parameters than PERC cells.

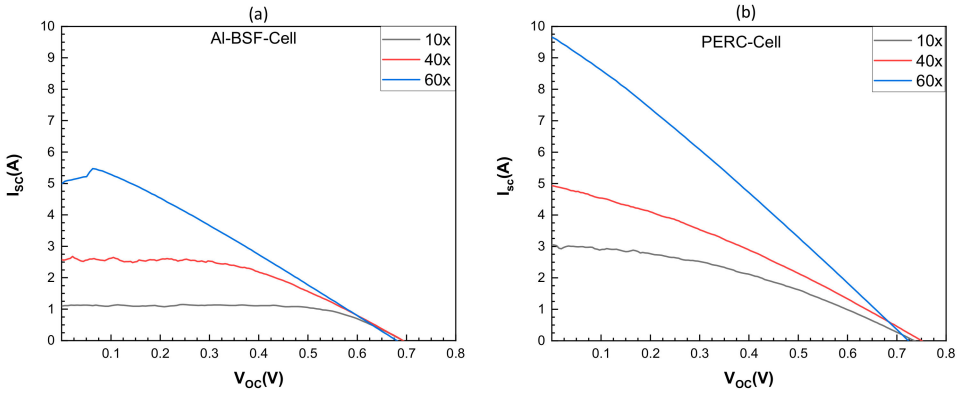

Figure 25. I–V curves for both Al-BSF (**a**) and PERC cell (**b**) under different concentrations.

6.3.2. Solar Simulator Test at Graz University of Technology

As mentioned above, the produced and laminated cells were also tested in a custom built high-flux solar simulator at Graz University of Technology (TUG) in order to verify the results obtained at GÜNAM and conduct tests with high spectral fidelity (Figure 26). A different type of lamp (i.e., metal-halide light source) and pure aluminum reflectors in combination with a silvered glass mirror light guiding tunnel were used. A detailed description of the spectral match and other solar simulator properties can be found in [35]. Also, note that only the Al-BSF cells, which seemed to reach higher efficiencies, were tested. The V_{OC} and I_{SC} results over varying concentration factors (25, 40, and 60 suns) are given in Figure 27.

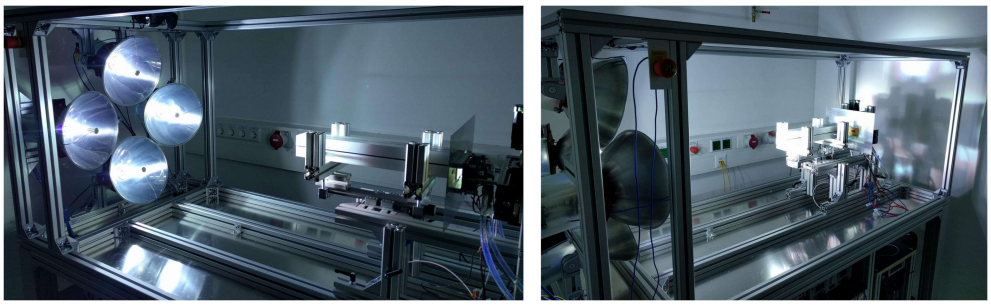

Figure 26. TUG's solar simulator test setup.

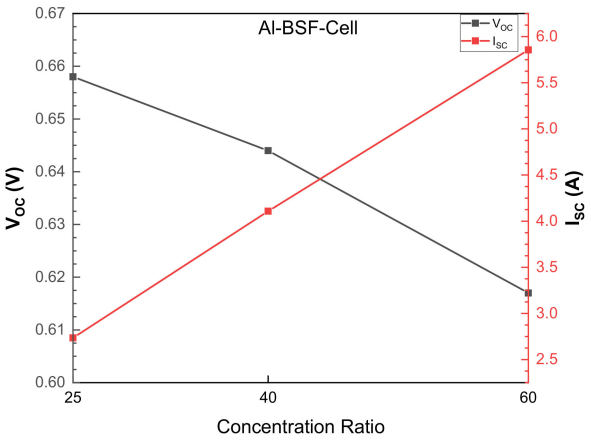

Figure 27. TUG high-flux solar simulator measurement results for V_{OC} and I_{SC} at varying concentration ratios.

The efficiencies of the cells presented in Table 3 are based on the active solar cell area of 1.6 × 2 cm^2 (which refers to the 2 × 2 cm^2 cell).

Table 3. Cell test at TUG's high-flux solar simulator at different concentration factors.

Irradiance (kW/m^2)	V_{OC} (V)	I_{SC} (A)	FF (%)	Efficiency (%)	Cell Temperature (°C)
25.5	0.658	2.735	0.752	16.6	26
40	0.644	4.108	0.730	15.1	31
60	0.617	5.855	0.698	13.1	35
80	0.587	7.533	0.661	11.4	38
101	0.552	9.053	0.640	9.9	43
111	0.529	9.362	0.724	10.1	44

During testing, the measurement system reached its maximum current limit at a concentration ratio exceeding 101 suns. This may have resulted in inaccurate maximum power point tracking. Therefore, the results obtained for 101 suns should be approached with caution.

However, the efficiency of the cells exhibited an approximately linear behavior between 25.5 and 80 suns. This indicates that the developed cells are a potentially viable solution and suitable for use under concentrated sunlight when considered as a low-cost alternative to multi-junction cells. It is important to note that the accuracy of the measurements can be affected by various factors, including the measurement system used and the concentration ratio. A thorough description of the measurement setup including uncertainty analyses can be found in [16]. Nevertheless, the data obtained from the experiments can provide valuable insights into the performance of the cells and their suitability for practical applications.

In order to determine the cell's temperature gradient, several measurements, as shown in Table 4, were performed. The average temperature coefficient was found to be −0.0693%(Abs)/K. While at first glance, the differences in temperature coefficient may vary depending on operating temperature, it is actually a nearly linear relation.

Table 4. Cell test at TUG's solar simulator at different junction cell temperature levels. The cell efficiency is related to the active solar cell area (2 cm × 1.6 cm).

Concentration Ratio (kW/m^2)	V_{OC} (V)	I_{SC} (A)	Efficiency (%)	Cell Temperature (°C)	Temperature Coefficient (%(Abs)/K)
61	0.612	5.896	12.9	35	-
61	0.579	5.930	11.8	51	−0.0698
61	0.540	5.937	10.2	70	−0.0801
61	0.521	5.920	9.7	80	−0.0579

Table 5 summarizes the most important KPIs (key performance indicators) of the Al-BSF CPV cells obtained through solar simulator measurements. The differences observed in the results may be attributed to the spectral characteristics of each solar simulator.

Table 5. The cells' performance parameters measured in the two different solar simulators at 60 suns.

	V_{OC} (V)	I_{SC} (A)	FF (%)	Efficiency (%)	Temperature (°C)
ODTÜ-GÜNAM	0.681	4.984	69.8	10.5	25
TUG	0.617	5.855	69.7	13.1	35

It was observed that the differences between the measurements taken at TUG and ODTÜ-GÜNAM solar simulators were significant. When tested in TUG's simulator, the same cells exhibited similar fill factors, but demonstrated higher efficiency compared to when they were tested in ODTÜ-GÜNAM's simulator, despite TUG's simulator operating under higher temperature. This suggests that factors other than temperature and radiation (e.g., potentially the spectral distribution of the simulators) significantly affect the performance of the CPV solar cells. In fact, the V_{OC} (open-circuit voltage) and I_{SC} (short-circuit current), which are both sensitive to spectral characteristics, differed between the two tests. By mapping the overlap between the cell's optimal light absorption and the spectrum emitted by the simulators, a more informed understanding of the cells' performance under different light sources can be obtained. However, detailed spectral distribution information is available only for TUG's solar simulator (also see [35]), as ODTÜ-GÜNAM's setup still needs to be characterized.

7. Discussion

7.1. Discrepancies between Simulation and Test Results

The manufacturing process of CPV cells involves critical parameters such as FF and various resistances that can significantly impact cell performance. Therefore, it is challenging to obtain optimal parameters in laboratory conditions during the manufacturing of CPV cells, and this often results in lower efficiency. As a result, the solar simulator testing conducted in the laboratory yielded lower efficiency than the simulation results.

Generally, CPV solar cell technology is designed to provide high efficiency, much like other solar technologies, while utilizing minimal area. The Griddler 2.5 PRO simulation results have been consistent with this expectation. However, it is important to note that the simulation results were achieved under ideal conditions and with optimum parameters, such as perfect metal printing quality. To improve the efficiency of proposed Al-BSF cells, the manufacturing process needs to be optimized, including the following:

- Optimizing metal printing quality: Precision in metal contacts is to be ensured to reduce electrical losses.
- Reducing various resistances: Sources of electrical resistance within the cell structure are to be minimized and design improvements and material enhancements should be implemented to decrease resistance.
- Improving Fill Factor (FF): Cell design is to be adjusted to effectively use space and enhance current flow and a balance between resistances is to be fine-tuned for the best FF.

7.2. Challenges in Manufacturing

The efficiency of CPV cells is affected by several manufacturing parameters, including thermal recombination on the surface and finger line resistance. To fully collect the expected high current, it is essential to increase the number of fingers. Additionally, it is necessary to increase the finger height to reduce the line resistance, since a delicate balance between active cell area and current carrying capacity is paramount. The introduction of more fingers, meant to bolster current carrying capacity, will inadvertently obscure the cell's active area, reducing sunlight absorption. This trade-off necessitates innovative solutions in material and design.

7.3. Finger Printing Issues

Screen printing was chosen as the primary manufacturing process to meet our desired goals. Concurrently, silver electroplating was also explored as an alternative manufacturing method. While defects in the fingers are known to be eliminated by silver electroplating and the finger height is increased, another problem was encountered: the silver did not adhere properly to the cell and would eventually detach, as shown in Figure 28. The issue of silver detachment during and after electroplating is a common problem in PV cell manufacturing. It can significantly impact the efficiency and performance of the cells. To overcome this

challenge, further research is needed to develop alternative manufacturing processes that can eliminate this problem and ensure the production of high-quality CPV cells. The use of advanced materials and manufacturing techniques may be necessary to achieve this goal.

Figure 28. Detachment of electroplated silver fingers and busbars.

In the case of CPV cells, electroplating can be a solution to achieve high current carrying capacity, but the process needs to be improved. Electroplating after screen printing can be replaced by laser ablation without prior screen printing. This change in the process can help to address the issue of silver detachment.

In industrial PV lines, small cells are not produced individually. In this case, they were separated by cutting the full wafer using an EO Technics Supermarker GF 311 nanosecond infrared (IR) laser (EO Technics, Seoul, Republic of Korea), which has a wavelength of 1064 nm and a maximum power of 30 W. Due to limitations of the available hardware, the edges of the cut cells could not undergo any passivation process, resulting in increased edge recombination observed as series resistance as well as reduced FF.

7.4. Module Assembly and Test Setup

Thirty-six of the 2 × 2 cm^2 Al-BSF CPV cells manufactured within this project were mounted on a special highly heat conducting PCB (CPV module), which is shown in Figure 29, for optimized heat rejection and tested under real-world outdoor conditions in a parabolic trough collector. The modules were attached to a highly optimized heat sink, which is essentially an absorber tube carrying a heat transfer fluid (HTF). Since the operating temperature of the c-Si CPV cells is limited to 98 °C, it is essential to ensure minimal thermal resistance between the cell and HTF. The heat sink and its design are described in detail in [36]. An image of the CPV module to be placed on the parabolic trough collector's absorber tube is given in Figure 30.

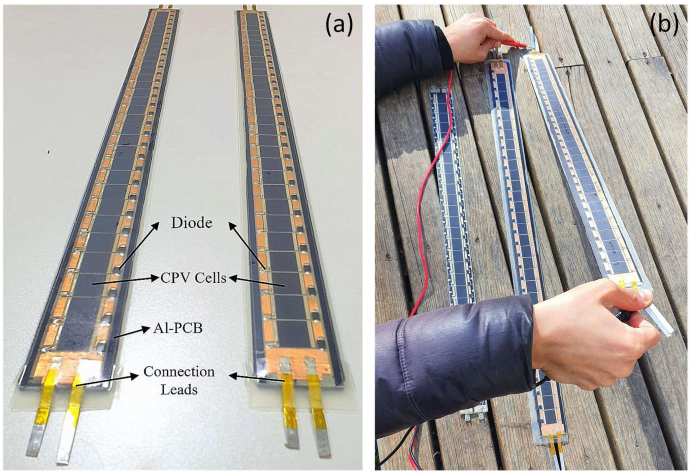

Figure 29. CPV module with custom made aluminum PCB (printed circuit board). (**a**) Close-up of the CPV cells mounted on the aluminum PCB, highlighting the key components. (**b**) First outdoor test of CPV cells under 1 sun.

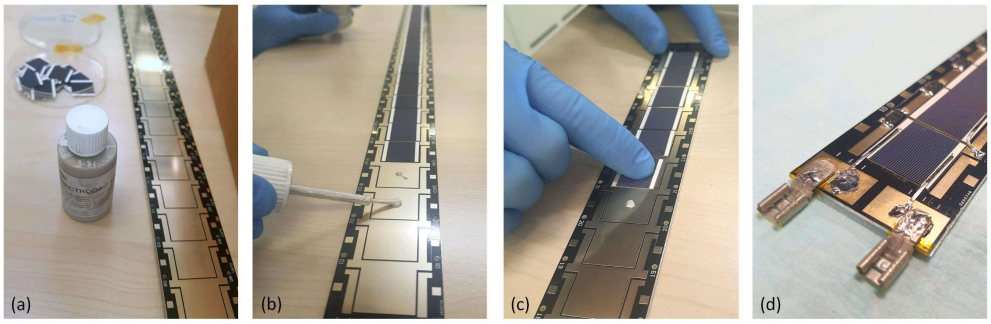

Figure 30. Connecting CPV cells with the commercial PCB. (**a**) initial parts and preparation stage (**b**) application of adhesive (**c**) placement of CPV cells (**d**) completed CPV circuit board assembly.

The cells used in this module are connected in series and a bypass diode is placed between every cell. This ensures that the efficiency of the entire module (shown in Figure 31) is not affected by suboptimal connections or cells or environmental effects such as partial shading or inhomogeneous illumination. By using bypass diodes, any cells that are not receiving sufficient sunlight can be bypassed to ensure that the efficiency of the module is maintained.

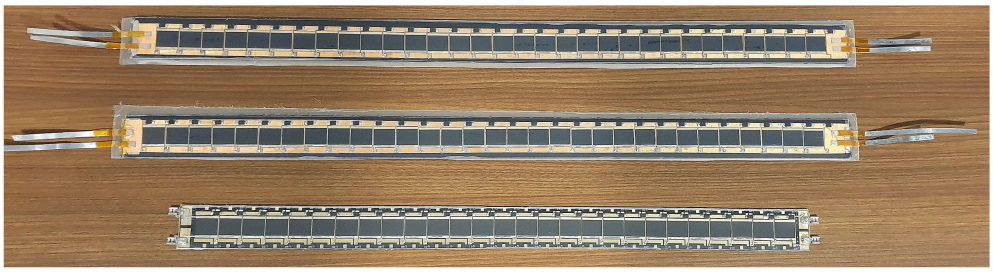

Figure 31. Images of the manufactured PV-PCB assembly.

8. Conclusions

Concentrating photovoltaics (CPVs) have shown great technological potential, particularly when used in CPV-T hybrid absorbers that allow for the recovery of waste heat for use as process heat. This paper has presented the development and testing of a low-cost alternative CPV cell based on c-Si for use in an injection-molded parabolic through a hybrid solar collector.

The study defined the target properties for the c-Si CPV cell based on the results of state-of-the-art analysis and evaluation of possible use cases for CPV-T heat and electricity use. Furthermore, two different c-Si cell technologies, namely, PERC and Al-BSF, were investigated, and the development of the cells, including simulation design and manufacturing, was described. The double-printing technique was used for finger production to reduce ohmic losses while carrying high currents under concentrated sunlight.

The study concluded that Al-BSF cells offer higher efficiencies than PERC cells for the designated use case. Solar simulator tests demonstrate that the cells can achieve efficiencies of 16.9% under 1 sun and 13.1% under 60 suns at 25 °C, with a temperature coefficient of −0.069%(Abs)/K. Highly doped cells (50 ohm/sq) with an area of about 4 cm^2 were eventually produced and assembled into a module of 36 cells. Finally, the produced cells were submitted to field testing at Graz University of Technology, as shown in Figures 32 and 33. Results of these tests will be published separately.

Figure 32. Photo of the CAM module installed in the parabolic trough collector for the first outdoor test operation.

Figure 33. Final test setup in Graz, Austria. The CAM is mounted in the parabolic trough collector. The electrical measurement and control system is located in a shelter (**left**). Parabolic mirror clamped onto the injection-molded support structure capable to follow the sun by two-axis tracking (**right**).

Overall, the development of a low-cost alternative CPV cell based on c-Si presents a viable option for lowering the cost of CPV-T hybrid absorbers.

Author Contributions: E.A.: writing—original draft, conceptualization; A.B.: writing—review and editing, project administration, funding acquisition; R.T.: resources; R.F.: data curation, investigation; R.P.: validation; A.A.: formal analysis; A.E.K.: methodology, validation; G.B.: methodology; B.A.: supervision. All authors have read and agreed to the published version of the manuscript.

Funding: This work was part of project ECOSun funded by the SOLAR-ERA.NET Cofund 2nd Call, managed by the Austrian Research Promotion Agency (FFG), FFG grant number 873785, supported by Open Access Funding by the Graz University of Technology. Authors affiliated with Graz University of Technology were responsible only for generating solar simulator results.

Data Availability Statement: The original contributions presented in the study are included in the article, further inquiries can be directed to the corresponding author.

Acknowledgments: Ertuğrul Çubuk, Deniz Değirmenci, İsmail Calayır, Murat Aynacıoğlu, Batuhan Dereli, Tayfun Yıldız, Mustafa Yalçın, Seda Kılıçkaya, Bülent Arıkan and Hasan Asav are kindly acknowledged.

Conflicts of Interest: The authors declare no conflicts of interest.

Nomenclature

Al–BSF	aluminum back surface field
CAM	co-generation absorber module
CPV	concentrated solar photovoltaic
CPV-T	concentrated photovoltaic and thermal hybrid system
CSP	concentrated solar power
c-Si	crystalline silicon
ECV	electrochemical capacitance voltage
EQE	external quantum efficiency
FF	fill factor
FPV	flat-plate photovoltaic
GPVL	ODTÜ-GÜNAM photovoltaic line
HTF	heat transfer fluid
J_{SC}	saturation current
LID	light-induced degradation
PERC	passive emitter rear contact
PV	photovoltaic
R_{CH}	characteristic resistance
R_S	series resistance
R_{SH}	shunt resistance
R_C	contact resistance
TLM	transmission line method
TUG	Graz University of Technology
V_{OC}	open-circuit voltage

References

1. Alexander, B.J.; Richardson, T.F. *Concentrating Solar Power Data and Directions for an Emerging Solar Technology*; Nova Science Publishers Inc.: Hauppauge, NY, USA, 2012.
2. Whitaker, C.M.; Dostalek, F.J. Performance of the EPRI high concentration photovoltaic module. In Proceedings of the Conference Record of the Twenty-Second IEEE Photovoltaic Specialists Conference, Las Vegas, NV, USA, 7–11 October 1991; Volume 1, pp. 512–517. [CrossRef]
3. Papis-Frączek, K.; Sornek, K. A Review on Heat Extraction Devices for CPVT Systems with Active Liquid Cooling. *Energies* **2022**, *15*, 6123. [CrossRef]
4. Aydin, E.; Tuncel, B.; Akinoglu, B.G. A Concentrating Mini Solar Power System to Overcome the Market Share. In Proceedings of the 2020 2nd International Conference on Photovoltaic Science and Technologies, PVCon, Ankara, Turkey, 30 November–2 December 2020. [CrossRef]
5. Youssef, W.B.; Maatallah, T.; Menezo, C.; Nasrallah, S.B. Assessment viability of a concentrating photovoltaic/thermal-energy cogeneration system (CPV/T) with storage for a textile industry application. *Sol. Energy* **2018**, *159*, 841–851. [CrossRef]
6. Felsberger, R.; Buchroithner, A.; Gerl, B.; Schweighofer, B.; Wegleiter, H. Design and testing of concentrated photovoltaic arrays for retrofitting of solar thermal parabolic trough collectors. *Appl. Energy* **2021**, *300*, 117427. [CrossRef]
7. Turkey's First Concentrated Solar Power Built in Southern City—HELIOSCSP. Available online: https://helioscsp.com/concentrated-solar-power-csp-technologies-status-and-analysis/ (accessed on 7 December 2023).
8. Concentrated Solar Power Had a Global Total Installed Capacity of 6451 MW in 2019. Available online: http://en.cnste.org/html/news/2020/0204/613.html (accessed on 7 December 2023).
9. Quaschning, V. Technical and economical system comparison of photovoltaic and concentrating solar thermal power systems depending on annual global irradiation. *Sol. Energy* **2004**, *77*, 171–178. [CrossRef]
10. Felsberger, R.; Buchroithner, A.; Gerl, B.; Schweighofer, B.; Preßmair, R.; Mitter, T.; Wegleiter, H. Optical performance and alignment characterization of a parabolic trough collector using a multi-junction CPV solar cell. *Sol. Energy* **2022**, *239*, 40–49. [CrossRef]
11. Felsberger, R.; Buchroithner, A.; Gerl, B.; Wegleiter, H. Conversion and Testing of a Solar Thermal Parabolic Trough Collector for CPV-T Application. *Energies* **2020**, *13*, 6142. [CrossRef]
12. Al-Maliki, W.A.K.; Khafaji, H.Q.A.; Wahhab, H.A.A.; Al-Khafaji, H.M.H.; Alobaid, F.; Epple, B. Advances in Process Modelling and Simulation of Parabolic Trough Power Plants: A Review. *Energies* **2022**, *15*, 5512. [CrossRef]
13. Green, M.A. Solar Cells: Operating Principles, Technology, and System Applications. 1982. Available online: https://ui.adsabs.harvard.edu/abs/1982ph...book.....G/abstract (accessed on 7 December 2023).
14. Ceballos, M.A.; Pérez-Higueras, P.J.; Fernández, E.F.; Almonacid, F. Tracking-Integrated CPV Technology: State-of-the-Art and Classification. *Energies* **2023**, *16*, 5605. [CrossRef]

15. Renno, C.; Petito, F. CPV System Optical Performance Evaluation by Means of Direct Experimental Measurement Procedure. *Energies* **2024**, *17*, 1288. [CrossRef]
16. El Himer, S.; El Ayane, S.; El Yahyaoui, S.; Salvestrini, J.P.; Ahaitouf, A. Photovoltaic Concentration: Research and Development. *Energies* **2020**, *13*, 5721. [CrossRef]
17. Renno, C.; Perone, A.; D'agostino, D.; Minichiello, F. Performance Evaluation of a Linear CPV/T System in Different Working Conditions. *Energies* **2023**, *16*, 2115. [CrossRef]
18. Liu, Y.; Hu, P.; Zhang, Q.; Chen, Z. Thermodynamic and optical analysis for a CPV/T hybrid system with beam splitter and fully tracked linear Fresnel reflector concentrator utilizing sloped panels. *Sol. Energy* **2014**, *103*, 191–199. [CrossRef]
19. Segev, G.; Kribus, A. Performance of CPV modules based on vertical multi-junction cells under non-uniform illumination. *Sol. Energy* **2013**, *88*, 120–128. [CrossRef]
20. Lokeswaran, S.; Mallick, T.K.; Reddy, K.S. Design and analysis of dense array CPV receiver for square parabolic dish system with CPC array as secondary concentrator. *Sol. Energy* **2020**, *199*, 782–795. [CrossRef]
21. Baig, H.; Heasman, K.C.; Mallick, T.K. Non-uniform illumination in concentrating solar cells. *Renew. Sustain. Energy Rev.* **2012**, *16*, 5890–5909. [CrossRef]
22. Malik, M.Z.; Shaikh, P.H.; Zhang, S.; Lashari, A.A.; Leghari, Z.H.; Baloch, M.H.; Memon, Z.A.; Caiming, C. A review on design parameters and specifications of parabolic solar dish Stirling systems and their applications. *Energy Rep.* **2022**, *8*, 4128–4154. [CrossRef]
23. Tawfik, M.; Tonnellier, X.; Sansom, C. Light source selection for a solar simulator for thermal applications: A review. *Renew. Sustain. Energy Rev.* **2018**, *90*, 802–813. [CrossRef]
24. Mellor, A.; Domenech-Garret, J.L.; Chemisana, D.; Rosell, J.I. A two-dimensional finite element model of front surface current flow in cells under non-uniform, concentrated illumination. *Sol. Energy* **2009**, *83*, 1459–1465. [CrossRef]
25. Despeisse, M.; Ballif, C.; Faes, A.; Lachowicz, A. Metallization and Interconnection for Silicon Heterojunction Solar Cells and Modules. *Photovolt. Int.* **2015**, *30*, 1–5.
26. Tepner, S.; Lorenz, A. Printing technologies for silicon solar cell metallization: A comprehensive review. *Prog. Photovolt. Res. Appl.* **2023**, *31*, 557–590. [CrossRef]
27. Mono p-Type Cells. Available online: https://www.heraeus.com/en/hpt/products_solutions_photovoltaics/silver_pastes/ptype_cells.html#tabs-307820-9 (accessed on 10 January 2024).
28. *G173-03*; Standard Tables for Reference Solar Spectral Irradiances: Direct Normal and Hemispherical on 37° Tilted Surface. ASTM International: West Conshohocken, PA, USA, 2020.
29. Compass. Available online: https://compass.astm.org/document/?contentCode=ASTM%7CG0173-03R20%7Cen-US&proxycl=https://secure.astm.org&fromLogin=true (accessed on 11 December 2023).
30. *AM1.5G*; Standard Solar Spectrum. ASTM International: West Conshohocken, PA, USA, 2020.
31. Almora, O.; Cabrera, C.I.; Garcia-Cerrillo, J.; Kirchartz, T.; Rau, U.; Brabec, C.J. Quantifying the Absorption Onset in the Quantum Efficiency of Emerging Photovoltaic Devices. *Adv. Energy Mater.* **2021**, *11*, 2100022. [CrossRef]
32. pv-Tools: TLM-SCAN+. Available online: http://www.pv-tools.de/products/tlm-scan/start-tlm.html (accessed on 8 December 2023).
33. Urban, T.; Miiller, M.; Heitmann, J. Full Analysis of Series Resistance Components and Their Degradation in Temperature Cycling of PERC Solar Cells. *AIP Conf. Proc.* **2022**, *2487*, 100003. [CrossRef]
34. Spi-Cell Tester?—Eternalsun Spire—PDF Catalogs | Technical Documentation | Brochure. Available online: https://pdf.directindustry.com/pdf/eternalsun-spire/spi-cell-tester/63104-605568.html (accessed on 10 January 2024).
35. Buchroithner, A.; Gerl, B.; Felsberger, R.; Wegleiter, H. Design and operation of a versatile, low-cost, high-flux solar simulator for automated CPV cell and module testing. *Sol. Energy* **2021**, *228*, 387–404. [CrossRef]
36. Santos, D.; Azgın, A.; Castro, J.; Kizildag, D.; Rigola, J.; Tunçel, B.; Turan, R.; Preßmair, R.; Felsberger, R.; Buchroithner, A. Thermal and fluid dynamic optimization of a CPV-T receiver for solar co-generation applications: Numerical modelling and experimental validation. *Renew. Energy* **2023**, *211*, 87–99. [CrossRef]